JCTC Journal of Chemical Theory and Computation

Article

pubs.acs.org/JCTC

Using Efficient Predictor-Corrector Reaction Path Integrators for Studies Involving Projected Frequencies

Hrant P. Hratchian*

Gaussian, Inc., 340 Quinnipiac Street, Building 40, Wallingford, Connecticut 06492, United States

ABSTRACT: Projected frequencies along a reaction pathway are necessary for computing reaction rates using variational transition state theory or reaction path Hamiltonian methods. The projected frequency analysis is quite sensitive to the accuracy of the reaction path integration. This work demonstrates that second- and first-order predictor−corrector reaction path integrators can be used for computing projected frequencies with high confidence. It is shown that these methods perform equally well with a variety of numerical integration step sizes and that, without a substantive loss in accuracy, Hessian updating can be used with both methods for stepping along the reaction path at points between those where projected frequencies are required.

1. INTRODUCTION

The steepest descent reaction path is the starting point for rate constant calculations using variational transition state theory (VTST), reaction path Hamiltonian (RPH), or related mechanistic models such as the Unified Reaction Valley Approach.[1−6] These approaches separate reaction dynamics into one classical translational degree of freedom along the reaction pathway and a set of transverse vibrational degrees of freedom treated quantum mechanically. Because the tangent of the reaction path at any point $\mathbf{x}(s)$ is given by the direction of the energy gradient at that point, VTST and RPH calculations are quite sensitive to the accuracy of the integrated reaction pathway.[7]

While a number of *reaction path* definitions have been developed, for the purposes of this work Fukui's intrinsic reaction coordinate (IRC) is taken as the reaction path definition.[8] The IRC is the curve in mass-weighted coordinates that begins at the reaction's transition structure (TS)—a first-order saddlepoint on the potential energy surface (PES)—and follows the two steepest-descent pathways downhill to the PES minima corresponding to reactant and product structures. Mathematically, the change in the nuclear geometry, $\mathbf{x}$, as a function of the arc length along the IRC, s, is given by

$$\frac{d\mathbf{x}}{ds} = -\frac{\mathbf{g}(\mathbf{x})}{|\mathbf{g}(\mathbf{x})|} \tag{1}$$

where $\mathbf{g}(x)$ is the energy gradient at $\mathbf{x}$.

When the magnitude of the gradient approaches zero, eq 1 can become stiff and difficult to integrate. When used in electronic structure studies, where the energy and derivatives can be computed on-the-fly as needed, it is advantageous to use an integrator that is accurate and robust so that the number of PES evaluations, which can be quite costly for some model chemistry choices, can be kept to a minimum. As a result, integration of reaction paths requires care, and a number of specialized integrators for this purpose have been developed.[9−36] Among these, the second-order implicit method of Gonzalez and Schlegel (GS2) is perhaps the most widely used.[29,30] This integrator employs a constrained optimization of each integration end-point to minimize the energy on a hypersphere of fixed radius. In practice, three to five minimization cycles—each involving energy and derivative evaluations—are typically required for each IRC point. This approach strikes an acceptable balance between cost and accuracy for reaction path following with electronic structure methods. Indeed, even for cases where the IRC is evaluated only to ensure that an optimized TS lies on a reaction pathway connecting intended PES minima, the GS2 integrator allows one to employ a relatively large step size and thereby requires a minimal number of energy and derivative evaluations. In such situations, it has also been shown that the GS2 scheme performs quite well with Hessian updating.[29] Taken together, this means that only energy and gradient computations are necessary, and the number of such evaluations is kept relatively small.

More recently, Burger and Yang developed a reaction path integrator that avoids the iterative optimization cycles of GS2 whenever possible by tracking the degree of stiff character in eq 1 during an IRC calculation.[31] When the reaction path is in a region of the PES where integration is difficult, the GS2 implicit method is used; in other regions of the path, an explicit integrator is employed. In this way, only a single evaluation is carried out in regions of the path where explicit integrators should perform well, while in more difficult portions a reliable, albeit somewhat more expensive, implicit method is used.

Another recent development in this area is the Hessian−based predictor−corrector (HPC) method of Hratchian and Schlegel.[33,34] This scheme combines the second-order local quadratic approximation (LQA) of Page and McIver[20,21] (predictor) with a modified Bulirsh−Stoer integrator (corrector).[33,37−39] Importantly, the corrector integration is carried out on a local fitted surface that is computationally free for studies using quantum chemical methods. Therefore, the total computational cost of the HPC integrator is the same as for

Special Issue: Berny Schlegel Festschrift

Received: May 19, 2012
Published: June 28, 2012

   dx.doi.org/10.1021/ct300407g | *J. Chem. Theory Comput.* 2012, 8, 5013−5019

LQA: one PES evaluation per IRC step. Hratchian et al. have also developed a first-order version of this integrator, referred to as Euler-based predictor−corrector (EulerPC).[35] An important advantage of EulerPC is that the $O(N_a^3)$ (where N_a is the number of atomic centers) computational work needed in the LQA and HPC methods is avoided. As a result, EulerPC has been shown to be an effective method for studies involving a very large number of nuclear degrees of freedom, such as macromolecular systems well-suited for studies with hybrid QM/MM model chemistries.[36]

In previous work, HPC was demonstrated to be at least as accurate as the GS2 integrator for computing reaction energy profiles and describing the dependence of geometric internal coordinates on the reaction coordinate. However, as noted by Schlegel,[40] the quality of the path tangent and projected frequencies is a much more sensitive test than the energy or coordinate profiles. In this report, two questions are explored. First, the accuracies of HPC and EulerPC methods are tested by computing projected frequency profiles along a particularly challenging reaction pathway. The robustness of these integrators is examined by studying how sensitive the accuracy of the projected frequency profile is to the integration step size. Since the computational cost differential between energy first and second derivatives using quantum chemistry models can be quite large, a second question asked here is whether analytic Hessian evaluations can be avoided at points where projected frequencies are not required. Such a scheme would minimize the cost of the IRC calculation while taking advantage of second-order information available from Hessians that must be computed irrespective of the IRC calculation (because they are needed for projected frequency analysis as part of a VTST or RPH computation). As is shown, HPC and EulerPC integrators perform quite well in both regards, suggesting that these approaches offer an excellent balance of cost and accuracy.

2. METHODS

This section begins with a brief description of the HPC and EulerPC methods. Then, an overview of the evaluation of projected frequencies along a reaction path is provided. For a complete treatment of HPC and EulerPC integrators, interested readers should consult previous papers.[33−35]

2.1. HPC and EulerPC Integrators. As with all predictor−corrector integrators,[41,42] HPC and EulerPC schemes are comprised of three coupled algorithmic elements: a predictor component (P), a function evaluation (E), and a correction step (C). HPC and EulerPC methods follow a P−E−C sequence. Both methods employ the same corrector scheme but differ in their P step definitions. The common C step uses energy and derivative information at the initial and final points from the P step, $\mathbf{x}_{i-1}$ and $\tilde{\mathbf{x}}_i$ (the tilde is used to distinguish the P end-point from the final predictor−corrector end-point, shown without a tilde), to fit a local analytic surface with which energy and gradient evaluations are affordable. Using this fitted surface, a modified Bulirsh−Stoer scheme[33,37−39] is used to carry out a more accurate integration from $\mathbf{x}_{i-1}$ to the final geometry in the P−E−C cycle, $\mathbf{x}_i$. Modified Bulirsh−Stoer integration requires first derivatives and involves an iterative scheme for determining the integration solution in the limit of a numerical step size of 0. This often requires a large number of first-derivative evaluations. The use of a fitted surface makes this otherwise computationally demanding approach essentially free in the context of electronic structure studies.

The quality of the corrector integration is tied to the accuracy of the fitted surface. The HPC and EulerPC methods incorporate modified Shepard interpolation.[43,44] The modified Shepard interpolation, or distance weighted interpolant (DWI) surface, is given by a weighted linear combination of second-order Taylor expansions. The fitted DWI energy at a point $\mathbf{x}$, $E_{DWI}(\mathbf{x})$, is always defined in terms of the initial and final points from the current P step:

$$E_{DWI}(\mathbf{x}) = w_{i-1}(\mathbf{x})\, T_{i-1}(\mathbf{x}) + w_{\tilde{i}}(\mathbf{x})\, T_{\tilde{i}}(\mathbf{x}) \tag{2}$$

The weighting functions, w_{i-1} and $w_{\tilde{i}}$, are given by

$$w_{i-1} = \frac{|\Delta\mathbf{x}_{\tilde{i}}|^2}{|\Delta\mathbf{x}_{i-1}|^2 + |\Delta\mathbf{x}_{\tilde{i}}|^2}$$
$$w_{\tilde{i}-1} = \frac{|\Delta\mathbf{x}_{x-1}|^2}{|\Delta\mathbf{x}_{x-1}|^2 + |\Delta\mathbf{x}_{\tilde{i}}|^2} \tag{3}$$

where $\Delta\mathbf{x}_{i-1} = \mathbf{x} - \mathbf{x}_{i-1}$ and $\Delta\mathbf{x}_{\tilde{i}} = \mathbf{x} - \tilde{\mathbf{x}}_i$. The Taylor expansions are given by

$$T_{i-1}(\mathbf{x}) = E_{i-1} + \mathbf{g}_{i-1}^t\Delta\mathbf{x}_{i-1} + \frac{1}{2}\Delta\mathbf{x}_{i-1}^t\mathbf{H}_{i-1}\Delta\mathbf{x}_{i-1}$$
$$T_{\tilde{i}}(\mathbf{x}) = E_{\tilde{i}} + \mathbf{g}_{\tilde{i}}^t\Delta\mathbf{x}_{\tilde{i}} + \frac{1}{2}\Delta\mathbf{x}_{\tilde{i}}^t\mathbf{H}_{\tilde{i}}\Delta\mathbf{x}_{\tilde{i}} \tag{4}$$

Subscripts $i-1$ and $\tilde{i}$ refer to points $\mathbf{x}_{i-1}$ and $\tilde{\mathbf{x}}_i$; E, $\mathbf{g}$, and $\mathbf{H}$ are the energy, gradient, and Hessian at the points indicated by each term's subscript. The computational bottleneck from the C step is the evaluation of quadratic terms in eq 4, which scales as $O(N_a^2)$. For EulerPC, the DWI surface evaluation presents the overall bottleneck for the reaction path integration; for HPC, the P component is more costly (*vide infra*).

The P component used in HPC integration is the LQA developed by Page and McIver.[20,21] Beginning with a quadratic expansion for the energy, eq 1 can be written as

$$\frac{d\mathbf{x}}{ds} = -\frac{\mathbf{g} + \mathbf{H}\Delta\mathbf{x}}{|\mathbf{g} + \mathbf{H}\Delta\mathbf{x}|} \tag{5}$$

Introducing the independent parameter t,

$$\frac{ds}{dt} = |\mathbf{g} + \mathbf{H}\Delta\mathbf{x}| \tag{6}$$

gives

$$\frac{d\mathbf{x}}{dt} = -[\mathbf{g} + \mathbf{H}\Delta\mathbf{x}] \tag{7}$$

Equation 6 can be used to numerically determine a Δt that corresponds to the desired IRC integration step of Δs in the current region of the PES. Given this Δt, eq 7 is used to take an LQA step. Numerical integration of both differential equations is done in the Hessian eigenvector space, which requires diagonalization of the force constant matrix. This represents the computational bottleneck of the LQA and HPC methods and scales as $O(N_a^3)$.

The predictor component of the EulerPC scheme is the simple first-order Euler method. In this case, the computational scaling of the P step is $O(N_a)$. Therefore, the overall scaling for EulerPC is dictated by the DWI surface evaluation work carried out as part of the C integration.

When either predictor−corrector method is used to take a step down the reaction path from point $\mathbf{x}_{i-1}$ to point $\mathbf{x}_i$, the P component involves taking a (LQA or Euler) step from $\mathbf{x}_{i-1}$ to

$\tilde{\mathbf{x}}_i$. Then, the (electronic structure) energy, gradient, and possibly Hessian are evaluated (the E component of the integrator) for $\tilde{\mathbf{x}}_i$. Using PES information from the initial and final P points, a local modified Shepard interpolated surface is formed.[43,44] With this fitted surface in hand, the modified Bulirsh−Stoer scheme is used to carry out a more accurate integration from $\mathbf{x}_{i-1}$ to the final point $\mathbf{x}_i$. The next HPC or EulerPC step is initiated with a new P step from the geometry given by $\mathbf{x}_i$ and the energy and gradient given at that point on the fitted surface used during the previous C step. On the basis of the reasonable assumption that $\tilde{\mathbf{x}}_i$ and $\mathbf{x}_i$ lie in the same quadratic region of the PES, the force constants at the two points are taken to be equivalent. This means that the Hessian used in the DWI expansion at the current initial P point was explicitly evaluated (analytically or using Hessian updating) at the previous P end-point. Also, in HPC integration the same Hessian is used during the LQA integration step to the new $\tilde{\mathbf{x}}$ point. Thus, electronic structure evaluations of the PES are only carried out at the TS and P end-points, $\mathbf{x}_0$ and $\tilde{\mathbf{x}}_i$. The result is that HPC and EulerPC calculations require only one quantum chemical calculation per requested IRC point.

2.2. Evaluation of Projected Frequencies. Expanding the (mass-weighted) Cartesian coordinates in the reaction path arc length gives

$$\mathbf{x}(s) = \mathbf{x}(0) + \mathbf{v}^0(0)s + \mathbf{v}^1(0)s^2 + \ldots \tag{8}$$

In eq 8, $\mathbf{v}^0(0)$ and $\mathbf{v}^1(0)$ are the reaction path tangent and curvature, respectively. These quantities can be written in terms of PES derivatives. Away from energy stationary points,

$$\mathbf{v}^0(s) = \frac{d\mathbf{x}}{ds} = -\frac{\mathbf{g}(\mathbf{x})}{|\mathbf{g}(\mathbf{x})|} \tag{9}$$

and

$$\mathbf{v}^1(s) = -\frac{\mathbf{H}\mathbf{v}^0 - (\mathbf{v}^{0t}\mathbf{H}\mathbf{v}^0)\mathbf{v}^0}{|\mathbf{g}(\mathbf{x})|} \tag{10}$$

Near stationary points, such as the TS, both expressions become ill-defined since the energy first derivatives vanish. At the TS, the tangent is given by the transition vector (the Hessian eigenvector corresponding to the imaginary frequency), and the curvature is

$$\mathbf{v}^1(s) = -[\mathbf{H} - 2(\mathbf{v}^{0t}\mathbf{H}\mathbf{v}^0)\mathbf{I}]^{-1}[\mathbf{F}^1\mathbf{v}^0 - (\mathbf{v}^{0t}\mathbf{F}^1\mathbf{v}^0)\mathbf{v}^0] \tag{11}$$

where $\mathbf{I}$ is the identity matrix ($I_{ij} = \delta_{ij}$) and $\mathbf{F}^1$ is a projection of the energy third derivatives ($F_{ijk} = (\partial^3 E)/(\partial x_i \partial x_j \partial x_k)$) on the reaction path tangent

$$F^1_{ij} = \sum_k F_{ijk} v^0_k \tag{12}$$

Projected frequency analysis is carried out by diagonalizing the Hessian after projecting into the subspace orthogonal to the reaction path. This projected Hessian, $\mathcal{H}$, is given by

$$\mathcal{H} = \mathbf{PHP} \tag{13}$$

The projection matrix, $\mathbf{P}$, is

$$\mathbf{P} = \mathbf{I} - \mathbf{v}^0\mathbf{v}^{0t} \tag{14}$$

When computing projected frequencies in this work, the tangent vector in eq 14 has been given by eq 9 at all points on the reaction path (except at the TS, where the transition vector is used).

As is done when integrating the path using HPC, projected frequency analysis along HPC and EulerPC reaction pathways is carried out applying the assumption that $\tilde{\mathbf{x}}_i$ and $\mathbf{x}_i$ lie in the same quadratic region of the PES. Thus, the Hessian at the P end-point ($\tilde{\mathbf{x}}_i$) is used for $\mathbf{H}$ in eq 13. The energy first-derivative vector used to define $\mathbf{v}^0$ is taken to be the gradient on the fitted DWI surface at $\mathbf{x}_i$, an approximation also applied in HPC and EulerPC propagation schemes. This allows projected frequency analysis along an HPC or EulerPC reaction pathway to be carried out as part of the IRC integration itself and provides the most cost-effective approach for such calculations. An alternative methodology would involve electronic structure calculations at each corrector end-point on the IRC. This would (at least) double the overall cost of the calculation. Preliminary studies indicate essentially no quantitative change in projected frequency profiles by using the former, more economical, scheme rather than the latter procedure.

3. RESULTS AND DISCUSSION

The symmetric S_N2 reaction of $Cl^- + H_3CCl \rightarrow ClCH_3 + Cl^-$ is used here as an example case. This test reaction has been used in other similar studies.[7,33,35] IRC integration for this reaction can be difficult due to the strong coupling of the high-frequency symmetric C−H stretch vibrational mode with the reaction coordinate.

All calculations have been carried out using a local development version of the Gaussian program suite.[45] The HF/6-31G(d) model chemistry has been employed throughout.[46−50] While this is a modest level of theory, it is adequate for the purposes of the present examination. The TS was optimized using very tight convergence criteria: 10^{-6} au for the root mean square (RMS) of the gradient; the threshold for the maximum absolute component of the gradient is 1.5 times larger; thresholds for the RMS and largest absolute element of the displacement vector are 4 times greater than the corresponding gradient thresholds.[51] When used, Hessian updating employs Bofill's method.[52]

Before considering HPC and EulerPC methods, it is useful to investigate the behavior of the LQA integrator. As outlined in section 2, the LQA method is employed as the predictor component of the HPC method. Note that simple Euler integration would serve the analogous purpose when considering EulerPC. Except for cases where the integration step size is quite small, Euler integration has very large errors in the path,[35] and, for this reason, results using Euler integration are not included in the present paper. For this reaction, it is known that second-order integrators reliably yield projected frequency profiles along the reaction coordinate for all but the C−H bond stretch mode (3423 cm^{-1} at the TS).[7] Therefore, the following discussion focuses on this specific projected frequency.

Figure 1 shows the symmetric C−H projected frequency as a function of the reaction coordinate based on paths determined by the LQA method with various integration step sizes. In the implementation used here, the initial step off the saddle point is equivalent to a Euler step following the Hessian eigenvector corresponding to the imaginary frequency. It is clear from the curves shown in the figure that this first step is rather poor. For the largest step size presented (Δs = 0.10 bohr amu^{-1}), the initial step results in an incorrect minimum in the projected frequency curve of nearly 25 cm^{-1}. Although the LQA integrator is eventually able to right itself in all cases, both

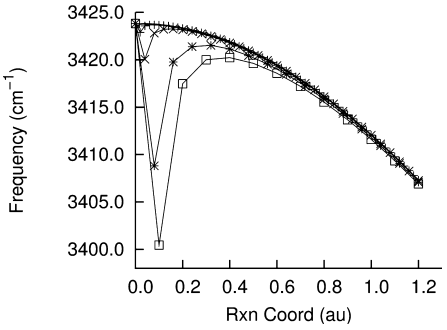

Figure 1. The symmetric C−H stretch projected frequency as a function of the reaction coordinate evaluated using the LQA method using analytic Hessians at all points. Numerical integrations with five different step sizes (in units of bohr amu$^{1/2}$) are included: 0.01 (solid line), 0.02 (+), 0.04 (×), 0.08 (∗); and 0.10 (□).

the magnitude of the error and the number of integration steps necessary to recover are strongly dependent on the step size.

For cases where projected frequencies are needed only every few IRC points, LQA may be less efficient than using a less accurate first-order integrator with a smaller step size. This consideration arises from the very different cost scaling of electronic structure first and second derivatives. If the LQA method could use Hessian updating for points between projected frequency analyses, the situation could be different. Then, it may be possible that LQA would take larger steps than an alternative first-order method without additional computational cost.

Figure 2 displays a test of such a scheme. Using integration step sizes of Δs = 0.04, 0.08, and 0.10 bohr amu$^{1/2}$, projected frequencies have been evaluated using analytic Hessians every 2, 3, 4, 5, and 10 IRC points; the force constants at integration steps between projected frequency analyses have been formed using Hessian updating. The results are somewhat promising. In all cases, the projected frequency curves approach the reference solution at large s. However, recovery from the error early in the reaction path is slower than in the cases using analytic Hessians at all integration steps. This is understandable since Hessian updating adds a layer of approximation to the method.

The data shown in Figures 1 and 2 suggest that, at least in the TS region, LQA may require very small integration steps in order to produce an IRC pathway accurate enough for projected frequency analysis. If VTST or RPH calculations require a fine grid of IRC points corresponding to a relatively small integration step, the LQA calculation does not present any additional computational effort. As Melissas et al. have pointed out,[53] this is not often the case. In that paper, it was suggested that LQA only be employed for small systems where the computational expense for second-derivative calculations is minimal. The results shown in Figure 1 support that conclusion, but Figure 2 indicates that the cost of Hessian evaluations at points where projected frequencies are not needed can be avoided by using Hessian updating. Although a smaller integration step size may be required, it is reasonable to expect that the appropriate step will be no smaller than that required by a first-order method.

Since the HPC integrator employs LQA as its predictor component, projected frequency profiles similar to those in Figure 1 provide a useful test of the fitted surface based modified Bulirsh−Stoer corrector scheme. Such a plot is shown

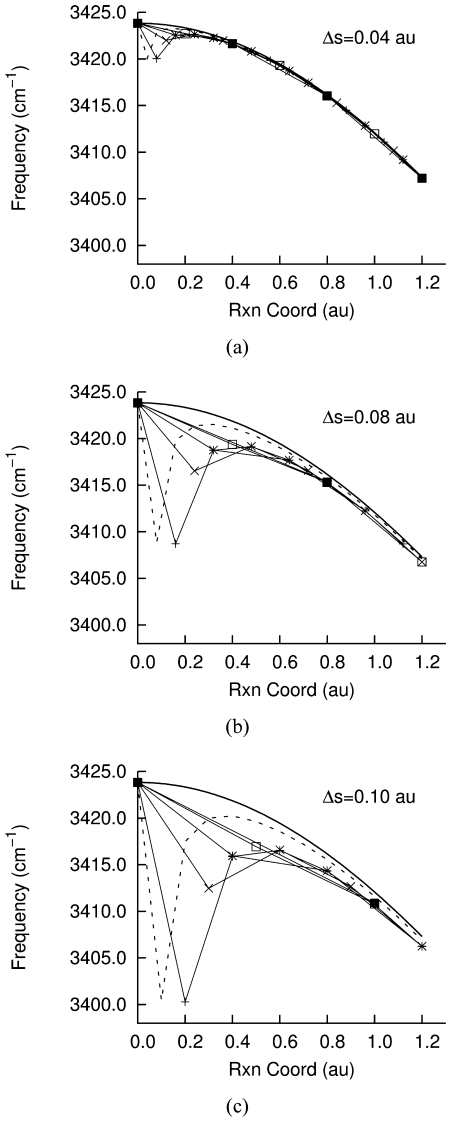

Figure 2. The symmetric C−H stretch projected frequency using LQA with analytic electronic structure Hessians evaluated at all steps (dashed line), every 2 (+), 3 (×), 4 (∗), 5 (□), and 10 (■) integration steps. Hessian updating was employed at intermediate steps. Three step sizes are shown: (a) 0.04, (b) 0.08, and (c) 0.10 bohr amu$^{1/2}$. The solid curve shows results using all analytic Hessians and Δs = 0.01 bohr amu$^{1/2}$. Projected frequency analysis was carried out at points with analytic Hessians.

in Figure 3. For all step sizes considered, the projected frequency profile follows the reference result almost perfectly. Clearly, the corrector integration is capable of righting the LQA errors. This critical improvement in integration quality is also robust with respect to integration step size. The projected frequency profiles for Δs = 0.01 bohr amu$^{1/2}$ and Δs = 0.10 bohr amu$^{1/2}$ are essentially indistinguishable in Figure 3.

EulerPC presents an even more stringent test of the corrector scheme since the errors in Euler integration are expected to be much more severe than for LQA. Nevertheless, EulerPC projected frequency profiles along the reaction coordinate appear to be as accurate as observed with HPC integration (see Figure 4). For all integration step sizes considered, the EulerPC profiles are nearly identical. The performance of the corrector integrator in these calculations is especially impressive. Again, the modified Bulirsh−Stoer

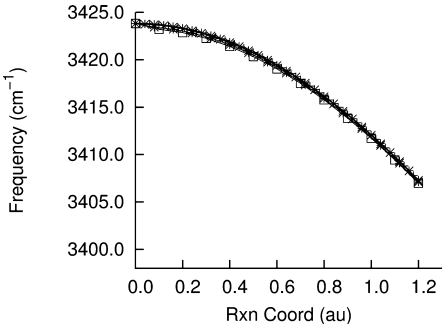

Figure 3. The symmetric C−H stretch projected frequency as a function of reaction coordinate evaluated using the HPC method using analytic Hessians at all points. Numerical integrations with five different step sizes (in units of bohr amu$^{1/2}$) are included: 0.01 (solid line), 0.02 (+), 0.04 (×), 0.08 (∗), and 0.10 (□).

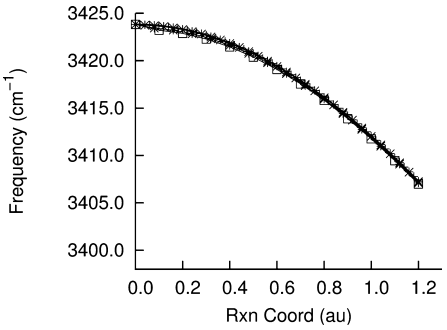

Figure 4. The symmetric C−H stretch projected frequency as a function of reaction coordinate evaluated using the EulerPC method using analytic Hessians at all points. Numerical integrations with five different step sizes (in units of bohr amu$^{1/2}$) are included: 0.01 (solid line), 0.02 (+), 0.04 (×), 0.08 (∗), and 0.10 (□).

scheme is able to make significant improvements to the predictor integration result. Importantly, the local fitted surface provides a quality representation of the PES, and these critical integration corrections are performed without additional computational overhead.

In Figure 2, it was shown that calculating the analytic Hessian every few LQA steps (for projected frequency analysis) and using Hessian updating at intermediate integration cycles does reasonably well at reproducing the all-analytic Hessian case, though some small differences are noticeable. The same test has been carried out using HPC and EulerPC methods, and the results are much improved. Figure 5 gives the outcome of these tests using HPC, and Figure 6 shows results from EulerPC calculations.

Two immediate observations can be made upon initial inspection of these two figures. First, Hessian updating does not degrade the refinement capability of the corrector scheme, and second, the quality of both HPC and EulerPC based projected frequency profiles remains mostly unaffected by Hessian updating. For both methods, essentially no deviation is observed using an integration step of Δs = 0.04 bohr amu$^{1/2}$. Using the larger Δs = 0.08 and Δs = 0.10 bohr amu$^{1/2}$ step sizes produces slight differences relative to the reference curve. Still, the HPC and EulerPC projected frequency profiles are qualitatively correct. More quantitatively, the maximum unsigned error for either integrator using a step size of 0.04 bohr amu$^{1/2}$ is 0.15 cm^{-1}; for Δs = 0.08 bohr amu$^{1/2}$, the

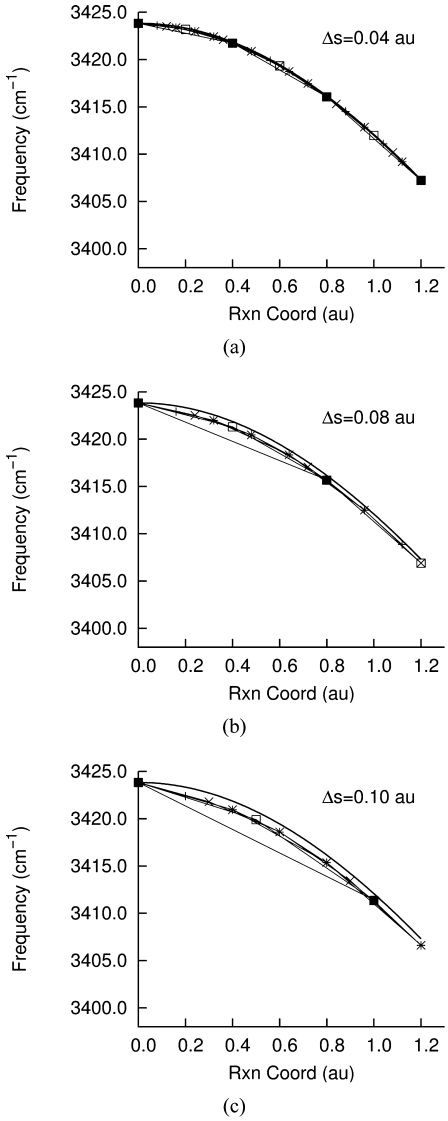

Figure 5. The symmetric C−H stretch projected frequency using HPC with analytic electronic structure Hessians evaluated every 2 (+), 3 (×), 4 (∗), 5 (□), and 10 (■) integration steps. Hessian updating was employed at intermediate steps. Three step sizes are shown: (a) 0.04, (b) 0.08, and (c) 0.10 bohr amu$^{1/2}$. The solid curve shows results using all analytic Hessians and Δs = 0.01 bohr amu$^{1/2}$. Projected frequency analysis was carried out at points with analytic Hessians.

maximum unsigned error is 0.61 cm^{-1}; for Δs = 0.10 bohr amu$^{1/2}$, the maximum unsigned error is 0.95 cm^{-1}.

4. CONCLUSIONS

This work investigated the use of HPC and EulerPC integration methods for generating reaction pathways used for projected frequency analysis. This type of analysis is necessary at multiple points along a reaction path when computing rate constants using methods such as VTST and RPH. Because the projected frequencies at a point on the PES depend on the reaction path tangent, their profile along the IRC is quite sensitive to errors in the reaction path integration. This is especially true when one or more transverse vibrational modes couple to the reaction coordinate.

The S_N2 reaction $Cl^- + H_3CCl \rightarrow ClCH_3 + Cl^-$ is known to be difficult for IRC integrators, and it was therefore chosen as a

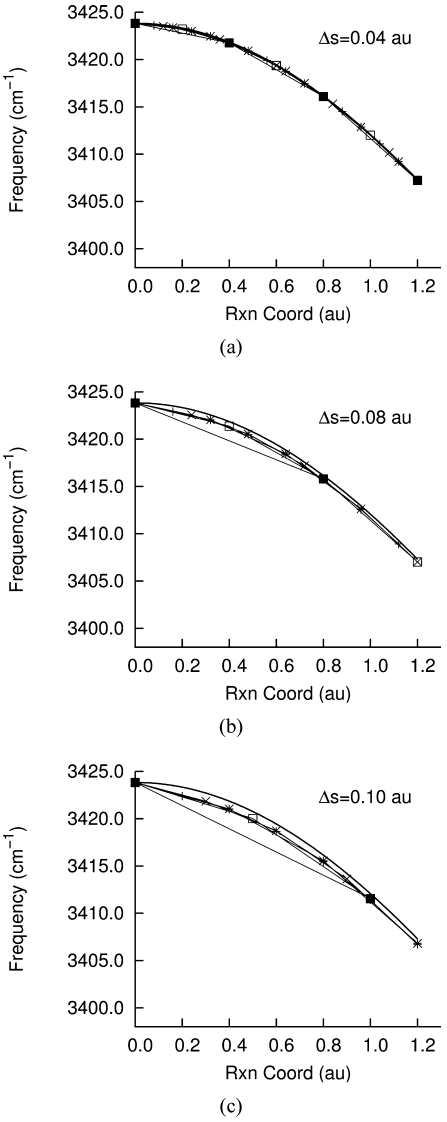

Figure 6. The symmetric C−H stretch projected frequency using EulerPC with analytic electronic structure Hessians evaluated every 2 (+), 3 (×), 4 (∗), 5 (□), and 10 (■) integration steps. Hessian updating was employed at intermediate steps. Three step sizes are shown: (a) 0.04, (b) 0.08, and (c) 0.10 bohr amu$^{1/2}$. The solid curve shows results using all analytic Hessians and Δs = 0.01 bohr amu$^{1/2}$. Projected frequency analysis was carried out at points with analytic Hessians.

challenging sample case in this study. In this example, the project frequency corresponding to the symmetric C−H stretch mode is strongly coupled to the reaction coordinate. It has been shown that errors in the TS region of the path using the second-order LQA integrator result in a deep artificial minimum in the symmetric C−H stretch profile. This error is dependent on the integration step size. With a step size of 0.02 bohr amu$^{1/2}$, the error is less than 2 cm^{-1}; with a step size of 0.10 bohr amu$^{1/2}$, the error grows to nearly 25 cm^{-1}. Conversely, HPC and EulerPC integrators yield profiles for this projected frequency that show only minor errors for any integration step size considered.

For studies where very accurate projected frequencies are desired at a relatively low density of points along the reaction path, this work has also shown that HPC and EulerPC integrators can use Hessian updating between steps where the frequency analysis is used. Such an approach can be carried out without compromising the observed accuracy compared to calculations using analytic second derivatives at all integration steps.

As a final note, it should be pointed out that the IRC pathway does not approximate the dynamics of chemical reactions exhibiting product branching. Therefore, it is often unphysical to use projected frequencies along such a path in kinetics and mechanistic models described earlier. In such cases, the IRC path heads downhill from the TS in a reaction valley until arriving at the branching, or valley−ridge inflection, point where the IRC continues along the ridge separating the minima valleys corresponding to branching products. (That the exact solution of eq 1 remains on the ridge is easily understood by observing that the negative Hessian eigenvector characterizing the valley−ridge inflection point is orthogonal to the path tangent.) Interestingly, if the second derivatives are known and diagonalized while following the IRC, as is the case when projected frequency analysis is being carried out, the onset of a valley−ridge inflection point is easily identified. Efficient new methods for locating branch points based on this observation may be considered in future work.

AUTHOR INFORMATION

Corresponding Author

*E-mail: hrant@gaussian.com.

Notes

The authors declare no competing financial interest.

ACKNOWLEDGMENTS

This work benefitted from insightful discussions with Prof. H. B. Schlegel (Wayne State University), whom the author is pleased to acknowledge and thank. Dr. M. Caricato (Gaussian, Inc.) is also thanked for helpful suggestions during the preparation of this paper.

REFERENCES

(1) Kraka, E.; Cremer, D. *Acc. Chem. Res.* **2010**, *43*, 591−601.
(2) Kraka, E. In *Encyclopedia of Computational Chemistry*; Schleyer, P. v. R., Allinger, N. L., Kollman, P. A., Clark, T., Schaefer, H. F., III, Gasteiger, J., Schreiner, P. R., Eds.; Wiley: Chichester, U. K., 1998; Vol. 2, pp 2437−2463.
(3) Garrett, B. C.; Truhlar, D. G. In *Encyclopedia of Computational Chemistry*; Schleyer, P. v. R., Allinger, N. L., Kollman, P. A., Clark, T., Schaefer, H. F., III, Gasteiger, J., Schreiner, P. R., Eds.; Wiley: Chichester, U. K., 1998; Vol. 2, pp 3094−3104.
(4) Truhlar, D. G.; Garrett, B. C.; Klippenstein, S. J. *J. Phys. Chem.* **1996**, *100*, 12771−12800.
(5) Truhlar, D. G.; Garrett, B. C. *Annu. Rev. Phys. Chem.* **1984**, *35*, 159−189.
(6) Miller, W. H.; Handy, N. C.; Adams, J. E. *J. Chem. Phys.* **1980**, *72*, 99−112.
(7) Baboul, A. G.; Schlegel, H. B. *J. Chem. Phys.* **1997**, *107*, 9413−9417.
(8) Fukui, K. *Acc. Chem. Res.* **1981**, *14*, 363−368.
(9) Schlegel, H. B. *WIREs Comput. Mol. Sci.* **2011**, *1*, 790−809.
(10) Hratchian, H. P.; Schlegel, H. B. In *Theory and Applications of Computational Chemistry: The First Forty Years*; Dykstra, C. E., Frenking, G., Kim, K. S., Scuseria, G. E., Eds.; Elsevier: Amsterdam, 2005; pp 195−249.
(11) Schlegel, H. B. *J. Comput. Chem.* **2003**, *24*, 1514−1527.
(12) Wales, D. J. *Energy Landscapes*; Cambridge University Press: Cambridge, U. K., 2003; pp 229−236.
(13) Schlegel, H. B. In *Encyclopedia of Computational Chemistry*; Schleyer, P. v. R., Allinger, N. L., Kollman, P. A., Clark, T., Schaefer Iii,

H. F., Gasteiger, J., Schreiner, P. R., Eds.; Wiley: Chichester, U. K., 1998; Vol. 4, pp 2432−2437.
(14) Collins, M. A. *Adv. Chem. Phys.* **1996**, *93*, 389−453.
(15) Schmidt, M. W.; Gordon, M. S.; Dupuis, M. *J. Am. Chem. Soc.* **1985**, *107*, 2585−2589.
(16) Ishida, K.; Morokuma, K.; Komornicki, A. *J. Chem. Phys.* **1977**, *66*, 2153−2156.
(17) Baldridge, K. K.; Gordon, M. S.; Steckler, R.; Truhlar, D. G. *J. Phys. Chem.* **1989**, *93*, 5107−5119.
(18) Garrett, B. C.; Redmon, M. J.; Steckler, R.; Truhlar, D. G.; Baldridge, K. K.; Bartol, D.; Schmidt, M. W.; Gordon, M. S. *J. Phys. Chem.* **1988**, *92*, 1476−1488.
(19) Aguilar-Mogas, A.; Gimenez, X.; Bofill, J. M. *Chem. Phys. Lett.* **2006**, *432*, 375−382.
(20) Page, M.; McIver, J. M. *J. Chem. Phys.* **1988**, *88*, 922−935.
(21) Page, M.; Doubleday, C.; McIver, J. W. *J. Chem. Phys.* **1990**, *93*, 5634−5642.
(22) Sun, J. Q.; Ruedenberg, K. *J. Chem. Phys.* **1993**, *99*, 5257−5268.
(23) Sun, J. Q.; Ruedenberg, K. *J. Chem. Phys.* **1993**, *99*, 5269−5275.
(24) Eckert, F.; Werner, H. J. *Theor. Chem. Acc.* **1998**, *100*, 21−30.
(25) Maluendes, S. A.; Dupuis, M. J. *J. Chem. Phys.* **1990**, *93*, 5902−5911.
(26) Hratchian, H. P.; Schlegel, H. B. *J. Phys. Chem. A* **2002**, *106*, 165−169.
(27) Mãijller, K.; Brown, L. D. *Theor. Chim. Acta* **1979**, *53*, 75−93.
(28) Gonzalez, C.; Schlegel, H. B. *J. Chem. Phys.* **1991**, *95*, 5853−5860.
(29) Gonzalez, C.; Schlegel, H. B. *J. Chem. Phys.* **1989**, *90*, 2154−2161.
(30) Gonzalez, C.; Schlegel, H. B. *J. Phys. Chem.* **1990**, *94*, 5523−5527.
(31) Burger, S. K.; Yang, W. T. *J. Chem. Phys.* **2006**, *124*, 224102.
(32) Burger, S. K.; Yang, W. T. *J. Chem. Phys.* **2006**, *125*, 244108.
(33) Hratchian, H. P.; Schlegel, H. B. *J. Chem. Phys.* **2004**, *120*, 9918−9924.
(34) Hratchian, H. P.; Schlegel, H. B. *J. Chem. Theory Comput.* **2005**, *1*, 61−69.
(35) Hratchian, H. P.; Frisch, M. J.; Schlegel, H. B. *J. Chem. Phys.* **2010**, *133*, 224101.
(36) Hratchian, H. P.; Frisch, M. J. *J. Chem. Phys.* **2011**, *134*, 204103.
(37) Bulirsch, R.; Stoer, J. *Num. Math.* **1964**, *6*, 413−427.
(38) Bulirsch, R.; Stoer, J. *Num. Math.* **1966**, *8*, 93−104.
(39) Bulirsch, R.; Stoer, J. *Num. Math.* **1966**, *8*, 1−13.
(40) Schlegel, H. B. *Faraday Discuss.* **1994**, *90*, 1569−1574.
(41) Gear, C. W. *Numerical Initial Value Problems in Ordinary Differential Equations*; Prentice-Hall: Englewood Cliffs, NJ, 1971.
(42) Press, W. H. *Numerical Recipes in FORTRAN 77: The Art of Scientific Computing*, 2nd ed.; Cambridge University Press: Cambridge, England, 1996; pp 701−744.
(43) Thompson, K. C.; Jordan, M. J. T.; Collins, M. A. *J. Chem. Phys.* **1998**, *108*, 564−578.
(44) Collins, M. A. *Theor. Chem. Acc.* **2002**, *108*, 313−324.
(45) Frisch, M. J.; Trucks, G. W.; Schlegel, H. B.; Scuseria, G. E.; Robb, M. A.; Cheeseman, J. R.; Scalmani, G.; Barone, V.; Mennucci, B.; Petersson, G. A.; Nakatsuji, H.; Caricato, M.; Li, X.; Hratchian, H. P.; Izmaylov, A. F.; Bloino, J.; Zheng, G.; Sonnenberg, J. L.; Liang, W.; Hada, M.; Ehara, M.; Toyota, K.; Fukuda, R.; Hasegawa, J.; Ishida, M.; Nakajima, T.; Honda, Y.; Kitao, O.; Nakai, H.; Vreven, T.; Montgomery, J. A., Jr.; Peralta, J. E.; Ogliaro, F.; Bearpark, M.; Heyd, J. J.; Brothers, E.; Kudin, K. N.; Staroverov, V. N.; Keith, T.; Kobayashi, R.; Normand, J.; Raghavachari, K.; Rendell, A.; Burant, J. C.; Iyengar, S. S.; Tomasi, J.; Cossi, M.; Rega, N.; Millam, J. M.; Klene, M.; Knox, J. E.; Cross, J. B.; Bakken, V.; Adamo, C.; Jaramillo, J.; Gomperts, R.; Stratmann, R. E.; Yazyev, O.; Austin, A. J.; Cammi, R.; Pomelli, C.; Ochterski, J. W.; Martin, R. L.; Morokuma, K.; Zakrzewski, V. G.; Voth, G. A.; Salvador, P.; Dannenberg, J. J.; Dapprich, S.; Parandekar, P. V.; Mayhall, N. J.; Daniels, A. D.; Farkas, O.; Foresman, J. B.; Ortiz, J. V.; Cioslowski, J.; Fox, D. J. *Gaussian Development Version*, revision H.20+; Gaussian, Inc.: Wallingford, CT, 2010.
(46) Ditchfield, R.; Hehre, W. R.; Pople, J. A. *J. Chem. Phys.* **1971**, *54*, 724−728.
(47) Hehre, W. J.; Ditchfield, R.; Pople, J. A. *J. Chem. Phys.* **1972**, *56*, 2257−2261.
(48) Gordon, M. S. *Chem. Phys. Lett.* **1980**, *76*, 163−168.
(49) Hariharan, P. C.; Pople, J. A. *Theor. Chim. Acta* **1973**, *28*, 213−222.
(50) Hariharan, P. C.; Pople, J. A. *Mol. Phys.* **1974**, *27*, 209−214.
(51) The optimized transition structure geometry used in this study belongs to the D_{3h} point group. The C and three H centers comprise the mirror plane. The C−H bond distance is 1.83814 Å and the C−Cl distance is 2.60867 Å.
(52) Bofill, J. M. *J. Comput. Chem.* **1994**, *15*, 1−11.
(53) Melissas, V. S.; Truhlar, D. G.; Garrett, B. C. *J. Chem. Phys.* **1992**, *96*, 5758−5772.